Electronic Supplementary Information

Experimental Section

Materials: Hydrochloric acid (HCl), ethanol (C_2H_5OH), potassium hydroxide (KOH), sodium chloride (NaCl), sodium carbonate (Na_2CO_3), N,N-diethyl-p-phenylenediamine (DPD), disodium phosphate (Na_2HPO_4), potassium phosphate monobasic (KH_2PO_4), sodium hydroxide (NaOH), ruthenium oxide (RuO_2), Pt/C (20 wt.%), cobalt nitrate hexahydrate ($Co(NO_3)_2·6H_2O$), iron nitrate nonahydrate ($Fe(NO_3)_3·9H_2O$), urea ($CO(NH_2)_2$), ammonium fluoride (NH_4F), and Nafion (5 wt.%), were purchased from Aladdin Ltd. (Shanghai, China). Sulfuric acid (H_2SO_4) and potassium permanganate ($KMnO_4$) were obtained from Beijing Chemical Reagent Co. Ltd. (Beijing, China). Tannic acid (TA) was purchased from Shanghai Maclin Biochemical Technology Co., Ltd. Ni foam (NF) was obtained from Shenzhen Green and Creative Environmental Science and Technology Co. Ltd. Natural seawater was collected from Qingdao, Shandong, China.

Preparation of CoFe LDH/NF and CoFe LDH@CoFe-TA/NF: Firstly, NF (2.0 × 3.0 cm^2) was pretreated by sonicating in HCl, ethanol, and water for 10 min, respectively. Then, the clean NF was immersed in a 30 mL mixed solution of $Co(NO_3)_2·6H_2O$ (0.15 g), $Fe(NO_3)_2·9H_2O$ (0.20 g), urea (0.61 g) and NH_4F (0.15 g), existing in a Teflon-lined autoclave. Subsequently, it was heated at 120 °C for 6 h. The CoFe LDH/NF was obtained after being washed and dried. And then, the prepared CoFe LDH/NF was immersed in TA (2 mg mL^{-1}) to acquire CoFe LDH@CoFe-TA/NF.

Preparation of RuO_2 on NF and Pt/C on NF: 5 mg RuO_2 was dispersed in mixed solution containing 30 μL of Nafion, 485 μL of ethanol, and 485 μL of water, and underwent sonicating for 30 min to form a homogeneous ink (5 mg mL^{-1}). 300 μL of catalyst ink was then dropped onto a piece of cleaned NF (1 × 0.5 cm^2) with a loading mass of 2.2 mg cm^{-2} to obtain RuO_2/NF. The preparation of the Pt/C/NF is similar to the preparation of RuO_2/NF, except that RuO_2 is replaced by Pt/C.

Characterizations: X-ray diffraction (XRD) data were gained using XRD, Philip D8. Scanning electron microscopy (SEM) images were acquired via SEM, ZISS 300

equipped with an energy dispersive X-ray (EDX) device. Transmission electron microscopy (TEM, JEM-F200, JEOL Ltd.) was utilized to further investigate the morphology of the catalyst. X-ray photoelectron spectroscopy (XPS) was implemented on an ESCALAB250 X-ray photoelectron spectrometer. UV-visible (UV-vis) spectrophotometry (Shimadzu UV-2700) was utilized for absorbance measurements.

Electrochemical evaluation: Electrochemical tests were operated in a standard three-electrode system with a CHI660E electrochemical workstation, in which the obtained materials, the Hg/HgO electrode and the carbon rod were used as the working electrode, the reference electrode and the counter electrode, respectively. Linear sweep voltammetry (LSV) was used to evaluate the catalytic activity with a scanning rate of 5 mV s^{-1}. The mentioned potentials are expressed against the reversible hydrogen electrode (RHE), which are converted according to the Nernst equation (E (vs. RHE) = E (vs. Hg/HgO) + 0.059 × pH + 0.098 V). The overpotential (η) of OER was calculated based on the formula η = E (vs. RHE) − 1.23 V, where 1.23 V is the thermodynamic OER potential. Tafel slope was obtained from the linear relationship between the overpotential and the logarithm of the corresponding current density (j).[1] In the frequency range of 0.01 to 1000,00 Hz, electrochemical impedance spectroscopy is tested. The drainage method was used to determine the Faraday efficiency of OER, which was carried out in a two-compartment H-type cell isolated by proton membranes. In order to visually demonstrate the corrosion resistance of the material, the corrosion polarization curve was also tested through the CHI660E electrochemical workstation. The iR-compensated potential ($E_{corr.}$) was calculated using the equation: $E_{corr.} = E - iR$, where E represents the original potential, R is the solution resistance, i is the corresponding current, and $E_{corr.}$ is the iR-compensated potential. All data have been reported with iR compensation except for the stability tests.

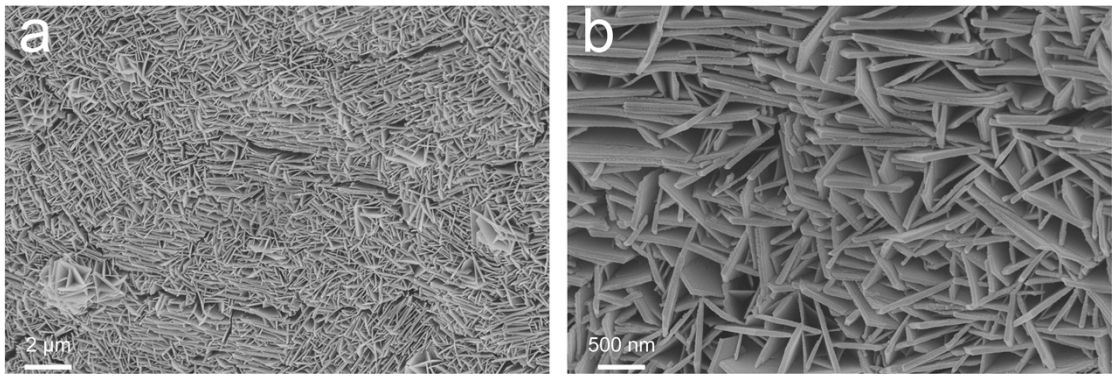

Fig. S1. (a) Low- and (b) high-magnification SEM images of CoFe LDH/NF.

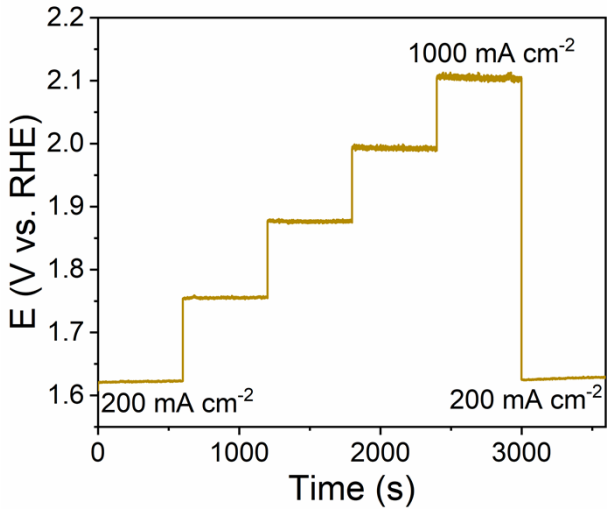

Fig. S2. Multistep chronopotentiometric curve of CoFe LDH@CoFe-TA/NF without iR correction in 1 M KOH.

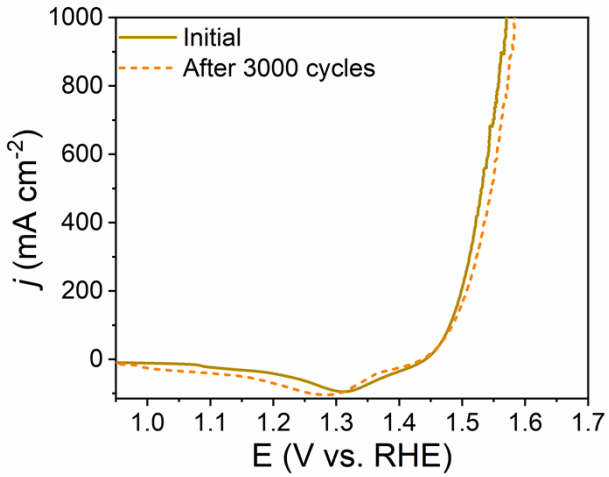

Fig. S3. LSV curves of CoFe LDH@CoFe-TA/NF before and after 3000 CV cycles in 1 M KOH.

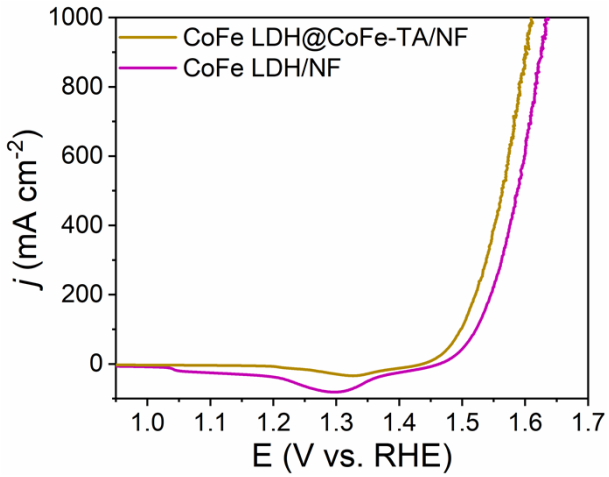

Fig. S4. LSV curves of CoFe LDH@CoFe-TA/NF and CoFe LDH/NF in 1 M KOH + seawater.

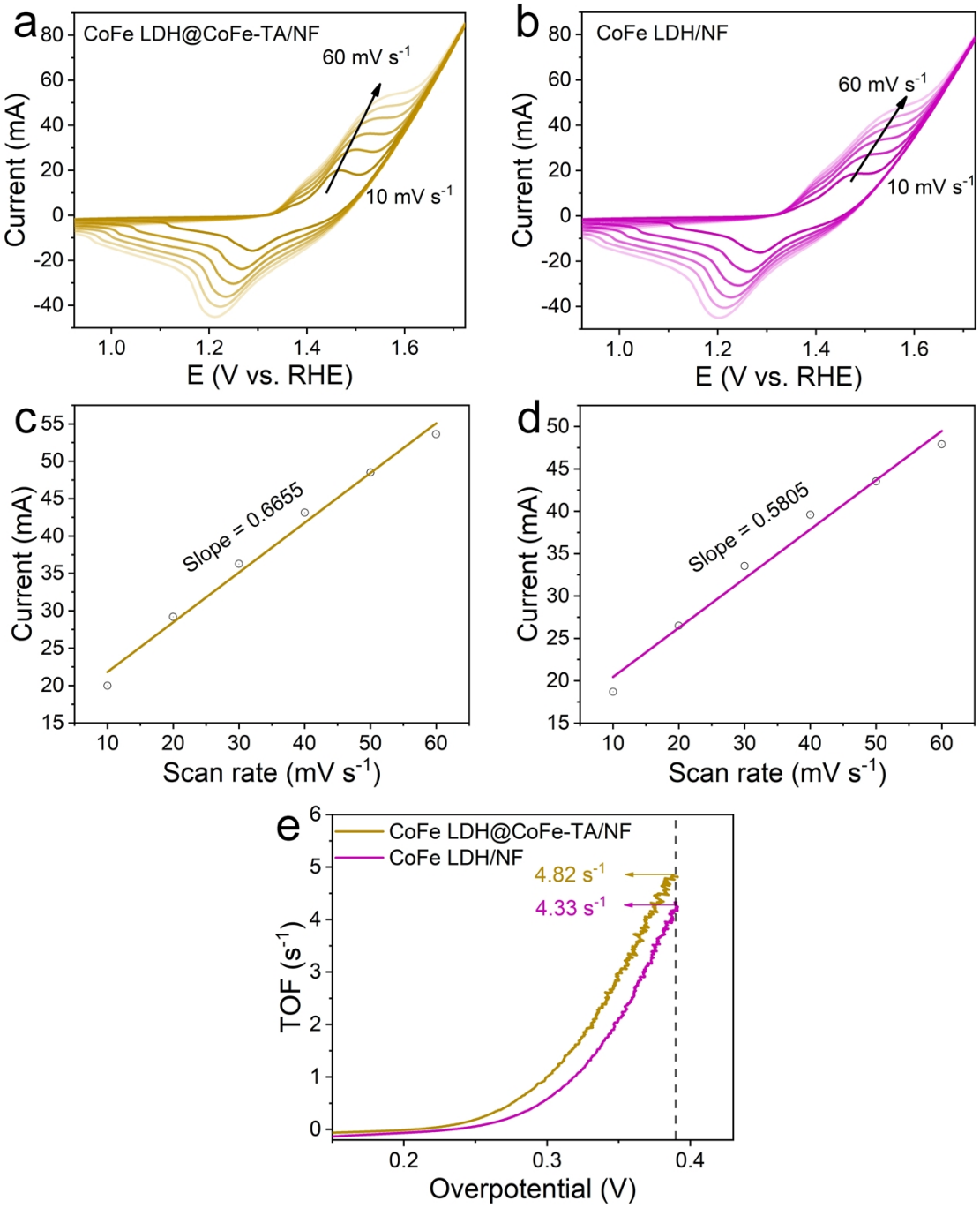

Fig. S5. CV curves for (a) CoFe LDH@CoFe-TA/NF and (b) CoFe LDH/NF at different scan rates increasing from 10 to 60 mV s^{-1} in 1 M KOH + seawater. Oxidation peak current vs. scan rate plot for (c) CoFe LDH@CoFe-TA/NF and (d) CoFe LDH/NF. (e) TOF plots of different samples.

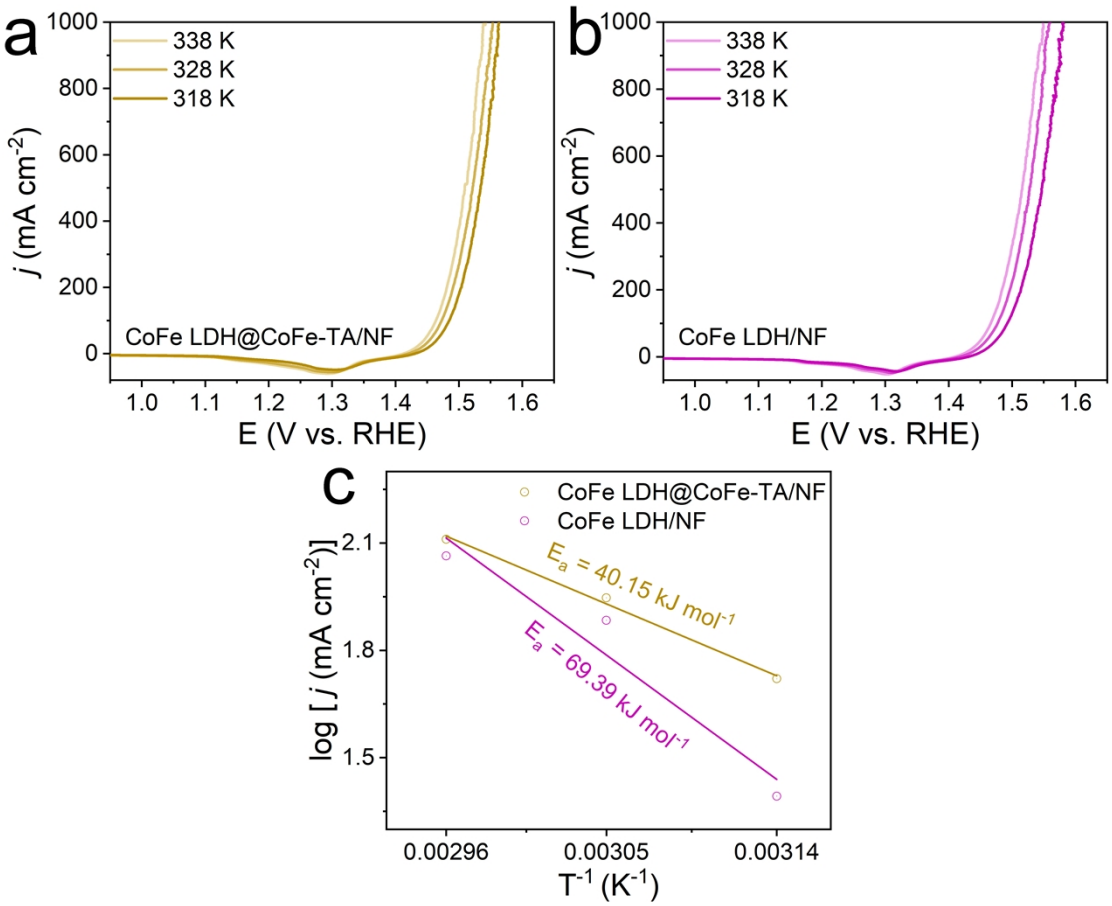

Fig. S6. LSV curves of (a) CoFe LDH@CoFe-TA/NF and (b) CoFe LDH/NF in 1 M KOH + seawater with different temperatures. (c) Arrhenius plots of the kinetic currents at 1.47 V vs. RHE for CoFe LDH@CoFe-TA/NF and CoFe LDH/NF.

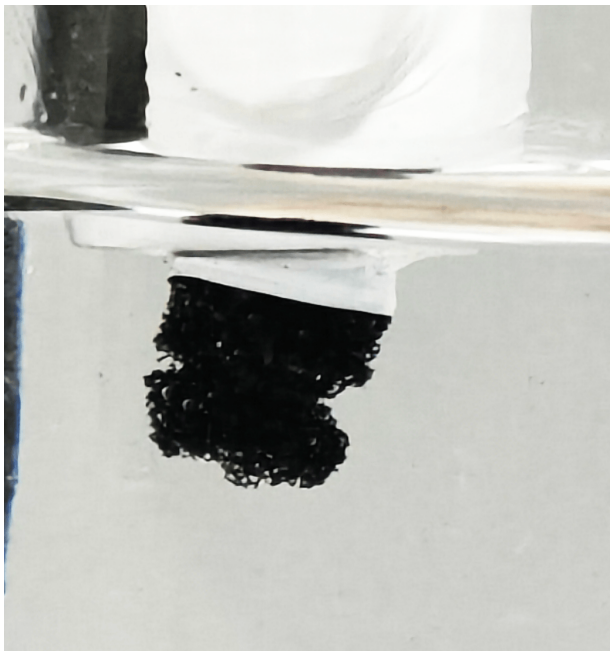

Fig. S7. Digital image of CoFe LDH/NF after durability test in 1 M KOH + seawater.

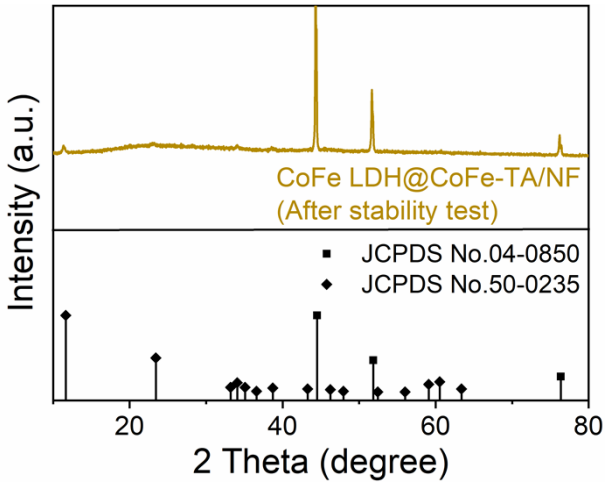

Fig. S8. XRD pattern of CoFe LDH@CoFe-TA/NF after stability test in 1 M KOH + seawater.

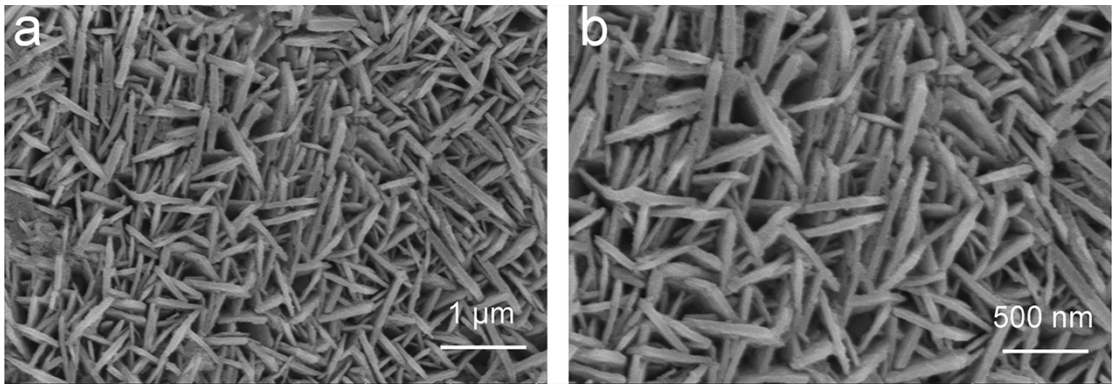

Fig. S9. (a) Low- and (b) high-magnification SEM images of CoFe LDH@CoFe-TA/NF after durable stability test in 1 M KOH + seawater.

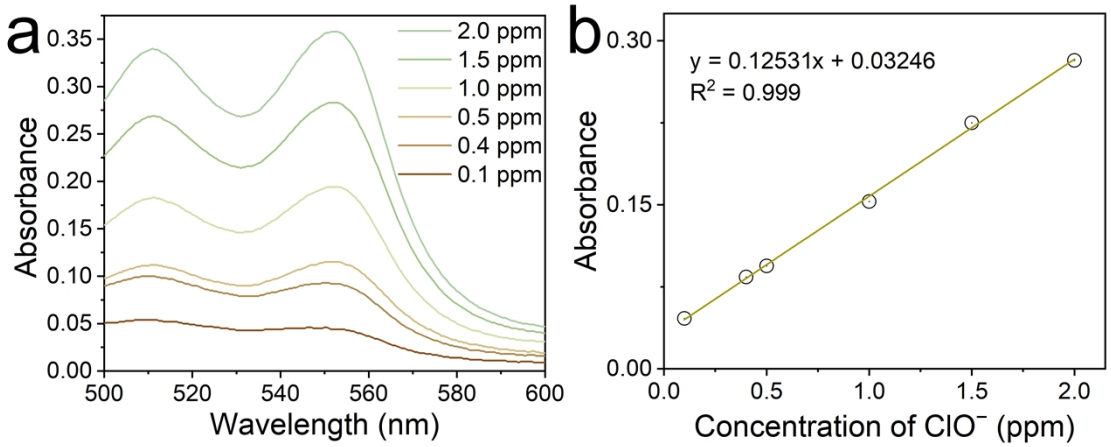

Fig. S10. (a) UV-vis absorption spectra of various active chlorine concentrations and (b) the corresponding linear fit.

Fig. S11. Photos showing color changes of CoFe LDH@CoFe-TA/NF and CoFe LDH/NF when potassium iodide and sodium thiosulfate were added to the electrolyte, respectively, after stability test at the *j* of 1000 mA cm^{-2} in 1 M KOH + seawater.

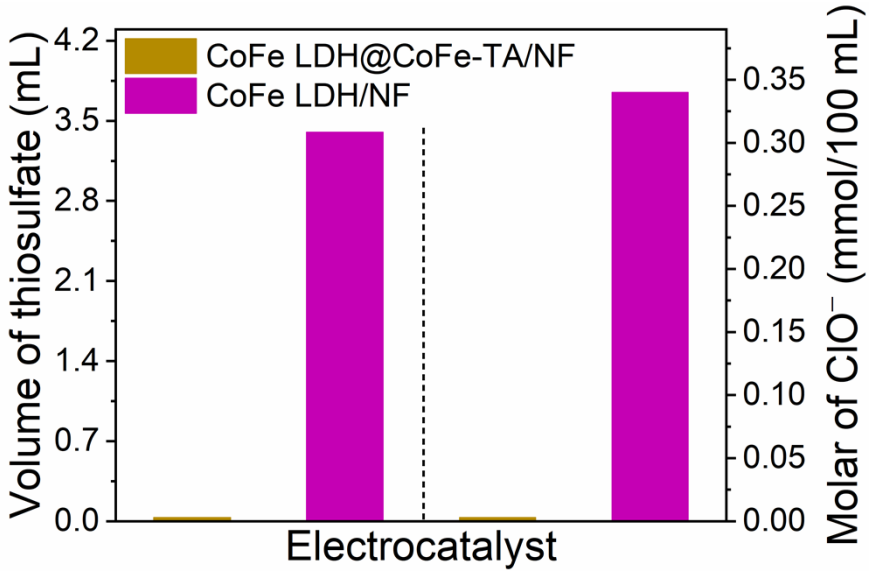

Fig. S12. The amount of thiosulfate consumed during the titration and the content of hypochlorite produced by CoFe LDH@CoFe-TA/NF and CoFe LDH/NF during the ASO process.

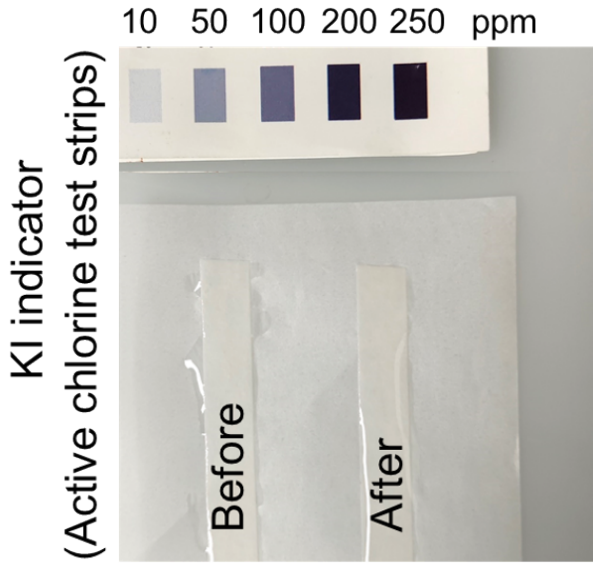

Fig. S13. Commercial test strip results of before and after stability test at the *j* of 1000 mA cm^{-2} in 1 M KOH + seawater.

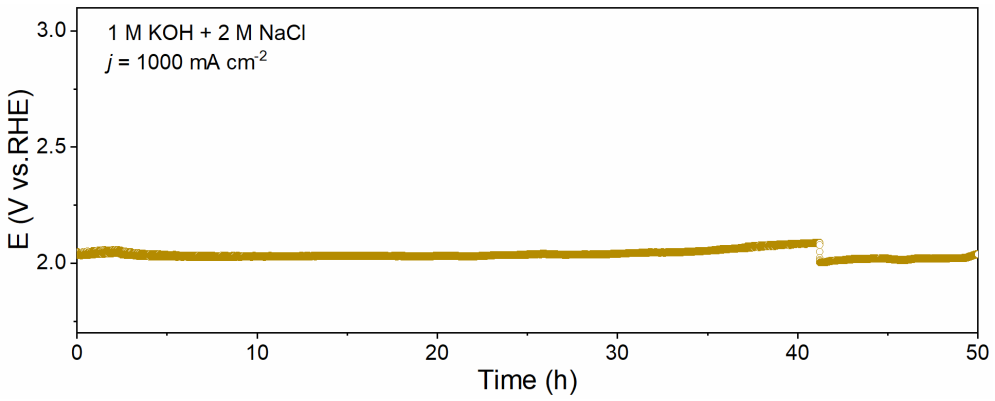

Fig. S14. Chronopotentiometric curve of CoFe LDH@CoFe-TA/NF at a *j* of 1000 mA cm^{-2} in 1 M KOH + 2 M NaCl.

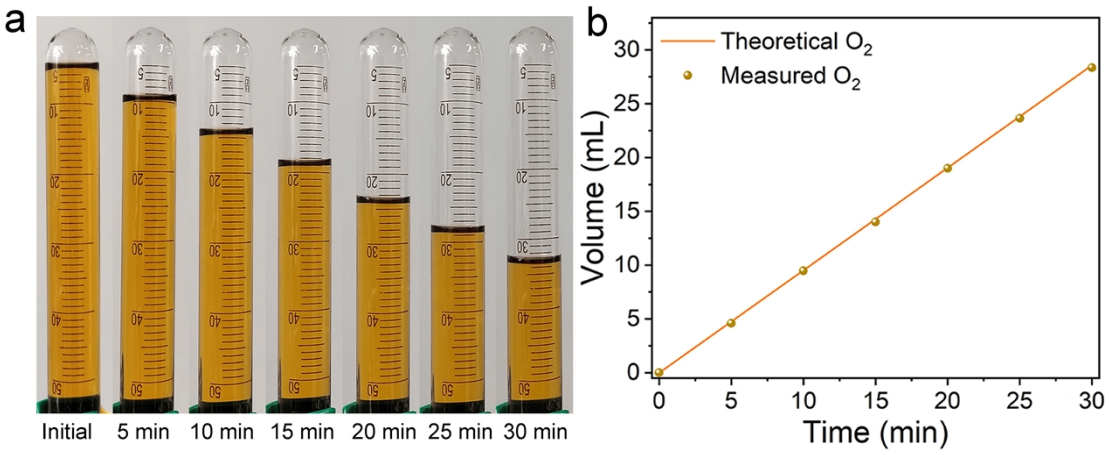

Fig. S15. (a) Collection of oxygen evolved from seawater oxidation at a *j* of 1000 mA cm^{-2} by water drainage method. (b) The volume of O_2, including calculated theoretically and measured experimentally.

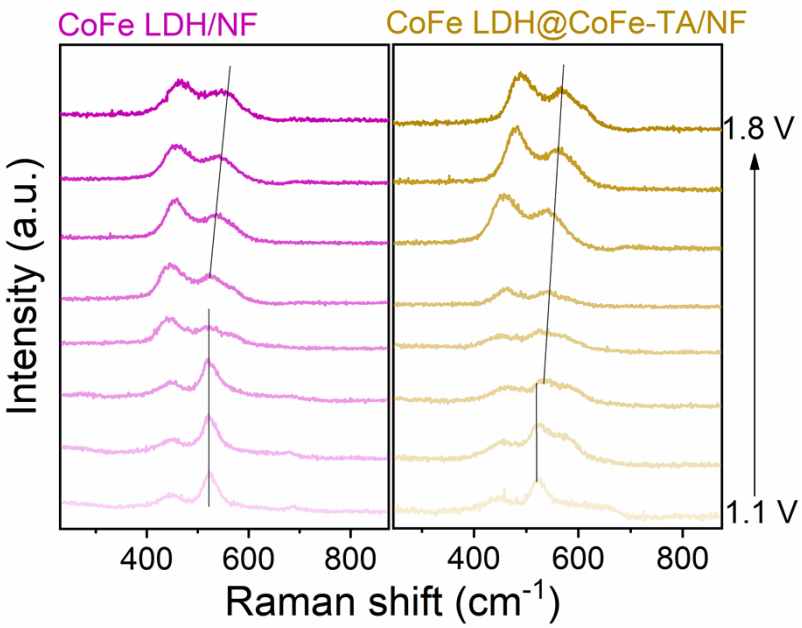

Fig. S16. In situ Raman data for CoFe LDH/NF and CoFe LDH@CoFe-TA/NF in 1 M KOH + seawater.

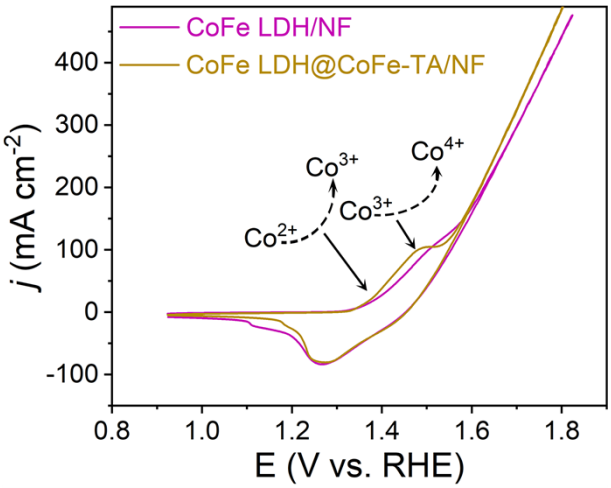

Fig. S17. CV curves of CoFe LDH@CoFe-TA/NF and CoFe LDH/NF at 10 mV s^{-1} in 1 M KOH + seawater.

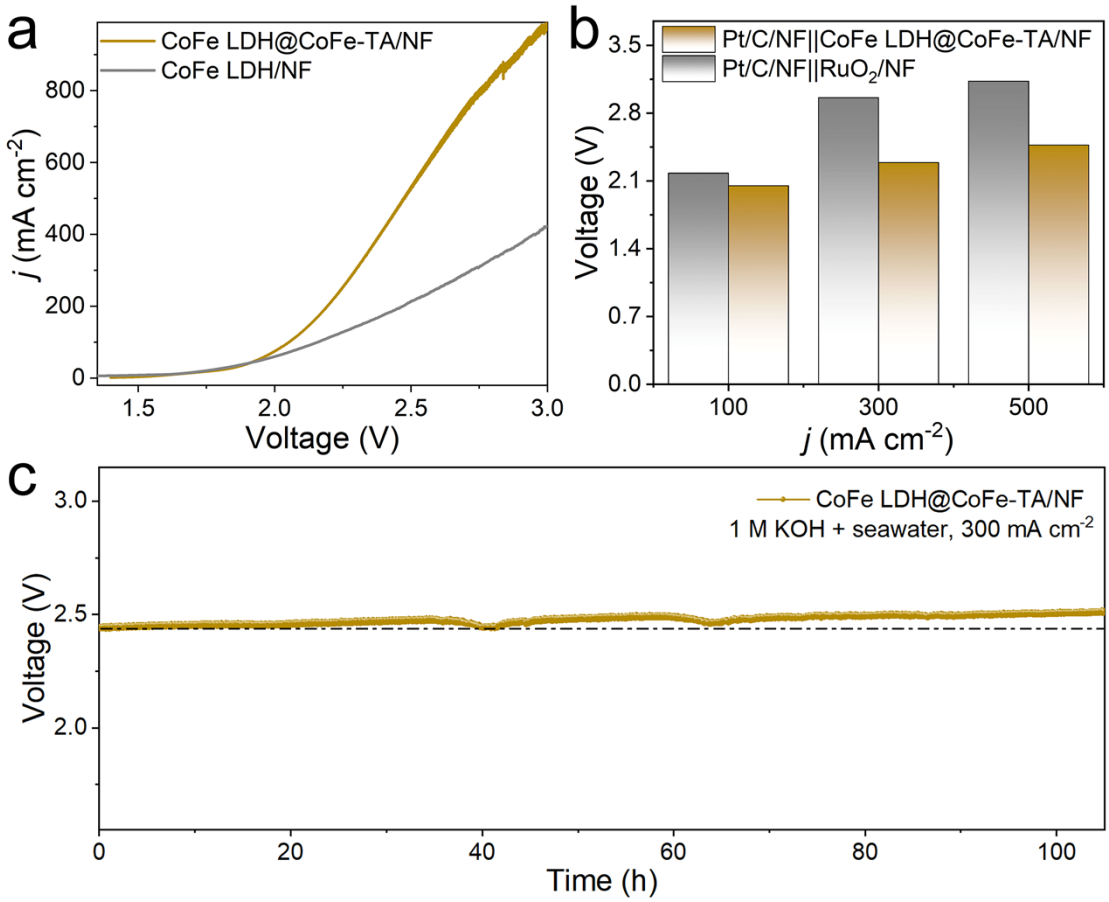

Fig. S18. (a) Polarization curves. (b) Cell voltages required for the two pairs of electrodes to achieve different *j*. (c) Chronopotentiometric curve of Pt/C/NF||CoFe LDH@CoFe-TA/NF at a *j* of 300 mA cm^{-2} in 1 M KOH + seawater in the MEA device.

Table S1. Comparison of electrochemical stability at different oxidation current densities for the CoFe LDH@CoFe-TA/NF with reported electrocatalysts in alkaline seawater.

Catalyst	Electrolyte	j (mA cm^{-2})	Time (h)	Ref.
CoFe LDH@CoFe-TA/NF	1 M KOH + seawater	1000	450	This work
NiFe LDH-CeW@NFF	1 M KOH + seawater	1000	100	2
Ni_3S_2/Fe-NiP_x/NF	1 M KOH + seawater	1000	35	3
MnCo/NiSe/NF	1 M KOH + seawater	500	200	4
B-Co_2Fe LDH/NF	1 M KOH + seawater	500	100	5
NiCo@NiFe LDH/NF	1 M KOH + seawater	500	100	6
Cr-CoFe LDH/NF	1 M KOH + seawater	500	100	7
CoP_x@FeOOH/NF	1 M KOH + seawater	500	80	8
$(Fe_{0.74}Co_{0.26})_2P$/Ni_3N	1 M KOH + seawater	500	40	9
CuO@CoFe LDH/CF	1 M KOH + seawater	200	50	10
Cr-Co_xP/NF	1 M KOH + seawater	100	140	11
NiCo LDH/NF	1 M KOH + seawater	100	100	12
NiFeCo LDH	1 M KOH + seawater	100	80	13
Fe-CoCH/NF	1 M KOH + seawater	100	50	14
Fe_2P/$Ni_{1.5}Co_{1.5}N$/Ni_2P	1 M KOH + seawater	100	40	15
$MnCo_2O_4$@NiFe LDH/NF	1 M KOH + seawater	100	25	16

Table S2. Leaching of each element for CoFe LDH@CoFe-TA/NF and CoFe LDH/NF after stability test in 1 M KOH + seawater.

Catalyst	Fe (ppm)	Co (ppm)
CoFe LDH@CoFe-TA/NF	0.004	0.004
CoFe LDH/NF	0.026	0.034

References

1. T. Shinagawa, A. T. Garcia-Esparza and K. Takanabe, Insight on Tafel slopes from a microkinetic analysis of aqueous electrocatalysis for energy conversion, *Sci. Rep.*, 2015, **5**, 13801.

2. M. Li, H. J. Niu, Y. Li, J. Liu, X. Yang, Y. Lv, K. Chen and W. Zhou, Synergetic regulation of CeO_2 modification and $(W_2O_7)^{2-}$ intercalation on NiFe-LDH for high-performance large-current seawater electrooxidation, *Appl. Catal. B Environ.*, 2023, **330**, 122612.

3. X. Luo, P. Ji, P. Wang, X. Tan, L. Chen and S. Mu, Spherical Ni_3S_2/Fe-NiP magic cube with ultrahigh water/seawater oxidation efficiency. *Adv. Sci.* 2022, **9**, 2104846.

4. R. Andaveh, A. S. Rouhaghdam, J. Ai, M. Maleki, K. Wang, A. Seif, G. B. Darband and J. Li, Boosting the electrocatalytic activity of NiSe by introducing MnCo as an efficient heterostructured electrocatalyst for large-current-density alkaline seawater splitting, *Appl. Catal. B Environ.*, 2023, **325**, 122355.

5. L. Wu, L. Yu, Q. Zhu, B. McElhenny, F. Zhang, C. Wu, X. Xing, J. Bao, S. Chen and Z. Ren, Boron-modified cobalt iron layered double hydroxides for high efficiency seawater oxidation, *Nano Energy*, 2021, **83**, 105838.

6. F. Zhang, Y. Liu, L. Wu, M. Ning, S. Song, X. Xiao, V. G. Hadjiev, D. E. Fan, D. Wang, L. Yu, S. Chen and Z. Ren, Efficient alkaline seawater oxidation by a three-dimensional core-shell dendritic NiCo@NiFe layered double hydroxide electrode, *Mater. Today Phys.*, 2022, **27**, 100841.

7. Y. Yao, C. Yang, S. Sun, H. Zhang, M. Geng, X. He, K. Dong, Y. Luo, D. Zheng, W. Zhuang, S. Alfaifi, A. Farouk, M. S. Hamdy, B. Tang, S. Zhu, X. Sun and W. Hu, Boosting alkaline seawater oxidation of CoFe-layered double hydroxide nanosheet array by Cr doping, *Small*, **2024**, 20, 2307294.

8. L. Wu, L. Yu, B. McElhenny, X. Xing, D. Luo, F. Zhang, J. Bao, S. Chen and Z. Ren, Rational design of core-shell-structured CoP@FeOOH for efficient seawater electrolysis, *Appl. Catal. B Environ.*, 2021, **294**, 120256.

9. W. Ma, D. Li, L. Liao, H. Zhou, F. Zhang, X. Zhou, Y. Mo and F. Yu, High-performance bifunctional porous iron-rich phosphide/nickel nitride heterostructures for alkaline seawater splitting, *Small*, 2023, **19**, 2207082.

10. X. Yang, X. He, L. He, J. Chen, L. Zhang, Q. Liu, Z. Cai, C. Yang, S. Sun, D. Zheng, A. Farouk, M. S. Hamdy, Z. Ren and X. Sun, A hierarchical CuO nanowire@CoFe-layered double hydroxide nanosheet array as a high-efficiency seawater oxidation electrocatalyst, *Molecules*, 2023, **28**, 5718.

11. Y. Song, M. Sun, S. Zhang, X. Zhang, P. Yi, J. Liu, B. Huang, M. Huang and L. Zhang, Alleviating the work function of vein-like Co_xP by Cr doping for enhanced seawater electrolysis, *Adv. Funct. Mater.*, 2023, **33**, 2214081.

12. R. An, G. Li and Z. Liu, Nickel-cobalt bimetal hierarchical hollow nanosheets for efficient oxygen evolution in seawater, *Materials*, 2024, **17**, 2298.

13. Y. S. Park, J. Y. Jeong, M. J. Jang, C. Y. Kwon, G. H. Kim, J. Jeong, J. H. Lee, J. Lee and S. M. Choi, Ternary layered double hydroxide oxygen evolution reaction electrocatalyst for anion exchange membrane alkaline seawater electrolysis, *J. Energy Chem.*, 2022, **75**, 127–134.

14. S. Shi, S. Sun, X. He, L. Zhang, H. Zhang, K. Dong, Z. Cai, D. Zheng, Y. Sun, Y. Luo, Q. Liu, B. Ying, B. Tang, X. Sun and W. Hu, Improved electrochemical alkaline seawater oxidation over cobalt carbonate hydroxide nanowire array by iron doping, *Inorg. Chem.*, 2023, **62**, 11746–11750.

15. F. Zhang, Y. Liu, F. Yu, H. Pang, X. Zhou, D. Li, W. Ma, Q. Zhou, Y. Mo and H. Zhou, Engineering multilevel collaborative catalytic interfaces with multifunctional iron sites enabling high-performance real seawater splitting, *ACS Nano*, 2023, **17**, 1681–1692.

16. N. Kitiphatpiboon, M. Chen, C. Feng, Y. Zhou, C. Liu, Z. Feng, Q. Zhao, A. Abudula and G. Guan, Modification of spinel $MnCo_2O_4$ nanowire with NiFe-layered double hydroxide nanoflakes for stable seawater oxidation, *J. Colloid Interface Sci.*, 2023, **632**, 54–64.